http://dx.doi.org/10.64837/GSA.13.1.5

Global and Stochastic Analysis
Vol. 13 No. 1 (2026)

Received: 01st October 2025 *Revised: 28th December 2025* *Accepted: 12th January 2026*

IMPACT OF GENERATION AND ABSORPTION OF HEAT ON THE FLOW OF BOGER FLUID PAST A CURVED STRETCHING SHEET: A NON-SIMILARITY SOLUTION APPROACH

S. SURESHKUMAR, K. M. DEVENDRAIAH*, S. PRASANNA RANI, C. G. JAGANNATHA, LAL SING NAIK AND K. C. JAGADEESHA*

Abstract. The objective of this effort is to provide a non-similar analysis of the heat transmission and flow of a Boger fluid past a curved stretched surface with the influence of a magnetic field. Boger fluids, on the other hand, are a class of viscoelastic fluids whose viscosity does not change significantly with changes in shear rate. Thanks to this property, they can have significant applications in the oil and gas industry, wherein they can be used to enhance the performance of drilling. Also, these fluids find use in constructing damping systems, which increases the safety and structural integrity of engineering installations. Additionally, exothermic and endothermic chemical reactions are used to investigate the characteristics of mass transport and heat. The curved stretchable surface has been subjected to convective conditions for mass and heat. The boundary layer equations are transformed into a non-similar form to enhance the precision and comprehensiveness of the analysis of flow, heat, and mass transport. The resultant non-similar partial differential equations (PDEs) are numerically solved using the local non-similarity approach by truncating up to the second level. Numerical data are presented graphically to examine the physical parameters' effects on flow, mass, and thermal transfer. It is important to note that when the solvent fraction parameter rises, the velocity profile rises as well. As the solutal and thermal Biot numbers climb, so does the temperature and concentration profile.

Nomenclature

Cp	Specific heat	R_1	Radius of curvature
a	Dimensional constant	ρ	Density
B_0	Magnetic field	(u, v)	Velocity components
ν	Kinematic viscosity	k	Thermal conductivity
(r_1, x)	Coordinates	D_B	Diffusivity
σ	Electrical conductivity	M	Magnetic parameter
Pr	Prandtl number	T	Temperature
Sc	Schmidt number	K	Boltzmann constant
h_s	heat transfer coefficient	Kr	Chemical reaction parameter

2000 *Mathematics Subject Classification.* Primary 76XX; Secondary 76A05, 76A10, 76Mxx.

Key words and phrases. Boger fluid; Magnetic field; Exothermic and Endothermic chemical reaction; Curved stretching sheet.

*Corresponding authors.

C	Concentration	K_r^2	The chemical reaction rate constant
h_m	Mass transfer coefficient	λ	Endothermic/exothermic reaction variable
E	Activation energy parameter	p	Pressure
δ	Temperature ratio	Δ	curvature parameter
β_2	The ratio of relaxation time	Bi_2	concentration Biot number
β_1	Solvent fraction parameter	Bi_1	Thermal Biot number
Ea	Activation energy	β^*	Heat of reaction

1. Introduction

Boger fluids, this type of viscoelastic liquid is almost linearly viscous as it deforms. Boger fluids do not shear-thin, as many polymeric fluids do, and nearly all of their viscosity remains constant when put under intense stretching or shear conditions. They are normally made by mixing a small amount of high-molecular-weight polymer with a highly viscous Newtonian solvent, e.g., corn syrup or the like, with little or no display of viscosity change. Due to such a special formulation, in the case of Boger fluids, the researchers have the opportunity to separate the effects of elasticity and changes in viscosity that depend on the shear during the experiment. They can easily test the effect of elasticity on the flow behavior by comparing the flow behavior of their fluids with that of Newtonian fluids whose viscosities are similar and gain a clearer picture of the non-Newtonian transport processes. Nagalakshmi and Vijaya [17] examined the motion of Boger nanoliquid via a Riga plate with Carbon nanotubes. Banakar et al. [4] inspected the flow of Boger nanofluid via a rotating rough disk. Abbas et al. [1] considered the nonlinear heat source impact on the stream of Boger liquid over a sheet. Mallikarjuna et al. [15] considered the motion of Boger fluid due to a slow-spinning disk with particle deposition effect. Panda et al. [19] elucidated the Boger-micropolar fluid flow through parallel disks. Habib et al. [8] analyzed the stream of Boger nanoliquid with the impact of the variable due to the revolution paraboloid.

Applications for flow analysis in the magnetic field (MF) presence are numerous in industries and engineering fields. A few examples are the design of cooling systems involving liquid metals, magnetohydrodynamic (MHD) generators, blood flow measurements, pumps, accelerators, and nuclear reactors. There is a lot of interest in the physiological mechanisms involved in MHD flow through an artery. Owing to these uses, scientists and researchers looked into MHD flows that corresponded to various physical properties. Banakar et al. [5] elucidated the unsteady fluid flow between two parallel active plates with the MF effect. Gowda et al. [21] scrutinized the impact of an MF on the flow of a nanofluid through a porous medium. Abbas et al. [2] conducted a study on the examination of heat transfer in a stretched flow caused by a curved surface, specifically in the occurrence of an MF. Banakar et al. [6] examined the movement of chemically reactive fluid past an off-center revolving disk with MF influence. Jagadha et al. [11] discussed the stream of Casson nanofluid with the MF impact via a revolving stretchy surface. Preethi et al. [20] elucidated the MHD effect on the motion of nanofluid through a stretchable surface.

An essential part of improving conventional fluid heat transmission is the chemical reaction. Thermal and mass transfer resulting from chemical reactions may be used in the

industrial sector to carry out significant engineering tasks, including drying and moisture distribution. In the majority of chemical reaction scenarios, the reactant concentration affects the response rate. When the rate of reaction and reactant concentration are exactly equal, a chemical reaction takes place. Chemical reactions fall into two categories: exothermic and endothermic. A heat-releasing process with a large negative enthalpy modification is called an exothermic reaction. Nonetheless, heat, light, or sound are frequently produced as byproducts of chemical processes. Heat is released into the environment as a result of exothermic processes. Chemical processes that absorb or utilize energy are referred to as endothermic. On the other hand, exothermic processes include iron rusting, thermite reaction, combustion, and burning sugar–water freezing. When reactant linkages break, endothermic reactions absorb more energy than is released when new bonds form in the products. The activation energy (AE) is the necessary energy required for chemical species, molecules, or atoms to initiate a reaction in a reactive system. Endothermic and exothermic chemical processes' effects on the stream of dusty fluid on a vertical surface were examined by Dey and Chutia [7]. In a convergent/divergent channel, the effect of exothermic-endothermic reactions and thermal energy was examined by Kouki et al. [13] on the flow of differential-type fluid. Using the Darcy–Forchheimer permeable space, Ullah [25] analyzed the impact of endothermic/exothermic reaction with AE. Sajid et al. [23] used the AE and convective boundary constraints to examine the consequence of exothermic/endothermic chemical processes on the flow of tri-hybrid nanofluids over the wedge. Sharma et al. [24] concentrated on the higher-order exothermic/endothermic chemical reaction on MHD flow through a stretching surface. Mansoor et al. [16] studied the chemical reaction impact on the flow of Williamson fluid via a non-linear stretching sheet.

The application of heat transfer and boundary layer flow over a stretched sheet in industry and industrial processes has garnered significant attention in recent times. These include the following processes: metal extrusion, hot rolling, glass fiber, wire drawing, metal spinning, continuous stretching of synthetic plastic films and fibers, and polymer extrusion. A curved jaw, used in basic extending assembly machinery, is an efficient way to employ liquid flow across a curved surface. Many studies on different fluid streams across the curved stretching sheets have been conducted recently. Jan et al. [12] used the non-similar analysis to study the dynamics of the magnetized flow of Reiner–Philippoff-based nanofluid via a CSS. Hayat et al. [9] considered the convective magnetite-Fe3O4 nanoparticles flow over a CSS. Veerannna et al. [26] inspected the performance of thermal transfer and flow of a Boger micropolar fluid over a CSS. Naveed et al. [18] scrutinized the micropolar fluid flow with thermal radiation past a CSS. Yasmin et al. [27] deliberated the mass and thermal transfer in the micropolar fluid flow due to a CSS. Imtiaz et al. [10] elucidated the Homogeneous-heterogeneous reaction's impact on second-grade fluid flow due to a CSS. Raza et al. [22] scrutinized the flow of Carreau liquid with the impact of non-linear thermal radiation over CSS.

It has been observed that in previous studies, a lot of emphasis has been placed on the boundary layer flow caused by CSS. Thus far, there has been no discussion on the exothermic and endothermic reactions in fluid flow caused by a CSS. In light of the previous discussion, the goal of this examination is to better comprehend the exothermic and endothermic reactions in the stream of Boger liquid via a CSS with the impact of MF and convective boundary conditions. The dimensional governing equations are reduced to non-dimensional non-similar PDEs with the aid of non-similarity transformations.

Using the local non-similarity technique yields a solution. To study the effects of diverse factors on the flow field, graphs are produced.

2. Mathematical formulation

Consider a two-dimensional flow of a Boger fluid caused by a CSS. The applied magnetic field's radial direction, with strength B_0, is considered. Fluid moves at a linear velocity ax along a curved surface with a curvature radius R_1, where a is a dimensional constant. Exothermic and endothermic chemical reactions are used to investigate the characteristics of mass transport and heat. There are mass and convective heat conditions are considered. Furthermore, it is believed that the hot fluid with a temperature T_w and concentration C_w, which result in mass and heat transfer coefficients of h_m and h_s, respectively, is heating the surface. The curvilinear coordinates (r_1, x) are used to simulate the governing equations

$$\frac{\partial}{\partial r_1}[v(r_1+R_1)]+R_1\frac{\partial u}{\partial x}=0, \tag{1}$$

$$\frac{u^2}{r_1+R_1}=\frac{1}{\rho}\frac{\partial P}{\partial r_1}, \tag{2}$$

$$\begin{aligned}\frac{uR_1}{r_1+R_1}\frac{\partial u}{\partial x}+v\frac{\partial u}{\partial r_1}+\frac{vu}{r_1+R_1}&=-\frac{\sigma B_0^2}{\rho}u-\frac{1}{\rho}\frac{\partial P}{\partial x}\frac{R_1}{r_1+R_1}\\&+\nu\frac{1+\beta_1}{1+\beta_2}\left(\frac{1}{r_1+R_1}\frac{\partial u}{\partial r_1}+\frac{\partial^2 u}{\partial r_1^2}-\frac{u}{(r_1+R_1)^2}\right)+g\beta_1(T-T_\infty),\end{aligned} \tag{3}$$

$$\begin{aligned}\frac{\partial T}{\partial x}\frac{uR_1}{r_1+R_1}+v\frac{\partial T}{\partial r_1}&=\frac{k}{(\rho Cp)}\left(\frac{1}{r_1+R_1}\frac{\partial T}{\partial r_1}+\frac{\partial^2 T}{\partial r_1^2}\right)\\&+K_r^2\frac{\rho\beta^*}{(\rho Cp)}\left(\frac{T}{T_\infty}\right)^n\exp\left(\frac{-E_a}{KT}\right)(C-C_\infty),\end{aligned} \tag{4}$$

$$\begin{aligned}v\frac{\partial C}{\partial r_1}+\frac{uR_1}{R_1+r_1}\frac{\partial C}{\partial x}&=D_B\left(\frac{\partial^2 C}{\partial r_1^2}+\frac{1}{R_1+r_1}\frac{\partial C}{\partial r_1}\right)\\&-K_r^2\left(\frac{T}{T_\infty}\right)^n\exp\left(\frac{-E_a}{KT}\right)(C-C_\infty).\end{aligned} \tag{5}$$

Boundary conditions (BCs):

$$\begin{aligned}&v=0, u=ax, -D_B\frac{\partial C}{\partial r_1}=h_m(C_w-C), -k\frac{\partial T}{\partial r_1}=h_s(T_w-T)\\&\frac{\partial u}{\partial r_1}\to 0, u\to 0, C\to C_\infty, T\to T_\infty.\end{aligned} \tag{6}$$

Non-similar transformations:

$$\begin{aligned}&\xi=\frac{x}{L}, \eta=r_1\sqrt{\frac{a}{\nu}}, \frac{C-C_\infty}{C_w-C_\infty}=\chi(\xi,\eta),\\&v=-\sqrt{\nu a}\frac{R_1}{R_1+r_1}\left(\frac{\partial}{\partial\xi}f(\xi,\eta)\xi+f(\xi,\eta)\right), u=ax\frac{\partial}{\partial\eta}f(\xi,\eta),\end{aligned}$$

$$\frac{T-T_\infty}{T_w-T_\infty}=\theta(\xi,\eta), p=\rho a^2x^2P(\xi,\eta). \tag{7}$$

Using equation (7), equations (1)–(5) are simplified as follows

$$P_\eta=\frac{1}{\eta+\Delta}f_\eta^2, \tag{8}$$

$$\begin{aligned}&\frac{1+\beta_1}{1+\beta_2}\left(-\frac{1}{(\eta+\Delta)^2}f_\eta+\frac{1}{(\eta+\Delta)}f_{\eta\eta}+f_{\eta\eta\eta}\right)\\&+(\xi f_\eta f_\xi+ff_\eta)\frac{\Delta}{(\eta+\Delta)^2}-Mf_\eta+\frac{Gr}{\xi}\theta-\frac{\Delta}{(\eta+\Delta)}(\xi f_\eta f_{\eta\xi}+f_\eta^2)\\&-\frac{\Delta}{(\eta+\Delta)}(2P+\xi P_\xi)+\frac{\Delta}{(\eta+\Delta)}(\xi f_{\eta\eta}f_\xi+ff_{\eta\eta})=0,\end{aligned} \tag{9}$$

$$\begin{aligned}&\frac{1}{\Pr}\left(\theta_{\eta\eta}+\frac{1}{(\eta+\Delta)}\theta_\eta\right)+\frac{\Delta}{(\eta+\Delta)}(\xi\theta_\eta f_\xi)+(f\theta_\eta)\frac{\Delta}{(\eta+\Delta)}\\&-\frac{\Delta}{(\eta+\Delta)}(\xi\theta_\xi f_\eta)+\lambda Kr(1+\delta\theta)^n\exp\left(\frac{-E}{(1+\delta\theta)}\right)\chi=0,\end{aligned} \tag{10}$$

$$\frac{1}{Sc}\left(\chi_{\eta\eta}+\frac{1}{(\eta+\Delta)}\chi_\eta\right)-\frac{\Delta}{(\eta+\Delta)}(\xi f_\eta\chi_\xi)+\frac{\Delta}{(\eta+\Delta)}(\xi\chi_\eta f_\xi) \tag{11}$$

$$+(f\chi_\eta)\frac{\Delta}{(\eta+\Delta)}-Kr(1+\delta\theta)^n\exp\left(\frac{-E}{(1+\delta\theta)}\right)\chi=0. \tag{12}$$

Reduced BCs:

$$f_\eta=1, f+\xi f_\xi=0, \theta_\eta=Bi_1(\theta-1), \chi_\eta=Bi_2(\chi-1).$$

$$f_\eta\to0, f_{\eta\eta}\to0, \theta\to0, \chi\to0, \tag{13}$$

where $M=\frac{\sigma B_0^2}{\rho a}$, $\Pr=\frac{\mu Cp}{k}$,$\Delta=R_1\sqrt{\frac{a}{\nu}}$, $\delta=\frac{T_w-T_\infty}{T_\infty}$, $\lambda=\frac{\beta^*}{Cp}\frac{C_w-C_\infty}{T_w-T_\infty}$, $Kr=\frac{K_r^2}{a}$, $E=\frac{Ea}{KT_\infty}$, $Bi_1=\frac{h_s}{k}\sqrt{\frac{\nu}{a}}$, $Bi_2=\frac{h_m}{D_B}\sqrt{\frac{\nu}{a}}$.

3. Solution Methodology

3.1. Local non-similarity approach. This approach's primary characteristic is its ability to produce nonsimilar solutions at any streamwise location without requiring the resolution of other streamwise sites. For computational simplicity, differential equations with an ordinary differential equation appearance are converted into localized solutions. Transformed coordinates ξ and η are chosen before physical coordinates x and r are swapped out. The η coordinate, which contains r, denotes pseudo-similarity. This function is constructed so that u is roughly denoted by $u\sim\frac{\partial f(\xi,\eta)}{\partial\eta}$. Furthermore, $\theta(\xi,\eta)$, a dimensionless temperature profile, is presented. When the transformation is performed to the conservation equations, the result is a set of differential equations that includes the standard set of η derivatives along with $\frac{\partial P}{\partial\xi}$, $\frac{\partial f}{\partial\xi}$, $\frac{\partial\theta}{\partial\xi}$ and $\frac{\partial\chi}{\partial\xi}$. Numerical techniques appropriate for handling PDEs must be applied in order to get the ξ derivatives during the solution phase. Moreover, the introduction of interdependencies between neighboring streamwise stations is an essential feature of the presence of ξ derivatives, this means that local independent solutions at distinct streamwise stations are no longer possible.

When terms involving $\frac{\partial}{\partial \xi}(\bullet)$ are excluded from the modified equations, they simplify the computation by becoming ordinary differential equations. By removing the streamwise link, this simplification makes it possible to arrive at locally independent solutions. This "local similarity" technology is beneficial for calculation, but it may yield results that are not entirely accurate.

In order to address the boundary layer flow problem across a CSS, the governing model found in Eqs. (8)–(11) and the BCs (13), the local non-similarity approach is utilized. The local non-similarity strategy for resolving the aforesaid problem will be described in depth in the next subsection (see refs. Liu et al. [14] and Afridi et al. [3]).

3.2. First-order truncation. Assuming that the $\xi\left(\frac{\partial(.)}{\partial \xi}\right)$ term is relatively small at the first level of truncation; it is assumed that $\xi \ll 1$ displays this behaviour. Because of this, Eqs. (8)–(11) take on the following forms:

$$P' = \frac{(f')^2}{\eta+\Delta}, \tag{13}$$

$$\left(-\frac{1}{(\eta+\Delta)^2}f_\eta + \frac{1}{(\eta+\Delta)}f_{\eta\eta} + f_{\eta\eta\eta}\right)\frac{1+\beta_1}{1+\beta_2} - Mf_\eta + \frac{Gr}{\xi}\theta - \frac{\Delta}{(\eta+\Delta)}(2P) + \frac{\Delta}{(\eta+\Delta)^2}(ff_\eta) + \frac{\Delta}{(\eta+\Delta)}(ff_{\eta\eta}) - \frac{\Delta}{(\eta+\Delta)}(f_\eta^2) = 0, \tag{14}$$

$$\frac{1}{\mathrm{Pr}}\left(\theta_{\eta\eta} + \frac{1}{(\eta+\Delta)}\theta_\eta\right) + \lambda(1+\delta\theta)^n Kr \exp\left(\frac{-E}{(1+\delta\theta)}\right)\chi + \frac{\Delta}{(\eta+\Delta)}(f\theta_\eta) = 0, \tag{15}$$

$$\frac{1}{Sc}\left(\chi_{\eta\eta} + \frac{1}{(\eta+\Delta)}\chi_\eta\right) - (1+\delta\theta)^n Kr \exp\left(\frac{-E}{(1+\delta\theta)}\right)\chi + \frac{\Delta}{(\eta+\Delta)}(f\chi_\eta) = 0. \tag{16}$$

The BCs are simplified as follows:

$$f' = 1, f = 0, \theta' = Bi_1(\theta - 1), \chi' = Bi_2(\chi - 1).$$
$$f' \to 0, f'' \to 0, \theta \to 0, \chi \to 0. \tag{17}$$

3.3. Second-order truncation. For truncation of higher order, introducing new functions $\frac{\partial P(\xi,\eta)}{\partial \xi} = q$, $\frac{\partial f(\xi,\eta)}{\partial \xi} = s$, $\frac{\partial \theta(\xi,\eta)}{\partial \xi} = t$, $\frac{\partial \chi(\xi,\eta)}{\partial \xi} = z$ are necessary to produce the 2nd order truncation. The ξ derivatives of the introducing function are set to zero that is $\frac{\partial q}{\partial \xi} = \frac{\partial s}{\partial \xi} = \frac{\partial t}{\partial \xi} = \frac{\partial z}{\partial \xi} = 0$. The modified Eqs. (8)–(13) are as follows

$$P' = \frac{(f')^2}{\eta+\Delta}, \tag{18}$$

$$\left(-\frac{1}{(\Delta+\eta)^2}f' + f''' + \frac{1}{(\Delta+\eta)}f''\right)\frac{1+\beta_1}{1+\beta_2} + \frac{\Delta}{(\eta+\Delta)^2}(ff' + \xi sf') - Mf' + \frac{Gr}{\xi}\theta - \frac{\Delta}{(\eta+\Delta)}((f')^2 + \xi s'f') + \frac{\Delta}{(\eta+\Delta)}(\xi sf'' + ff'') = \frac{\Delta}{(\eta+\Delta)}(2P + \xi q), \tag{19}$$

$$\frac{1}{\mathrm{Pr}}\left(\theta'' + \frac{1}{(\eta+\Delta)}\theta'\right) + \frac{\Delta}{(\eta+\Delta)}(\xi s\theta') + \frac{\Delta}{(\eta+\Delta)}(f\theta') - \frac{\Delta}{(\eta+\Delta)}(\xi f' t) + \lambda Kr(1+\delta\theta)^n \exp\left(\frac{-E}{(1+\delta\theta)}\right)\chi = 0, \tag{20}$$

$$\frac{1}{Sc}\left(\chi'' + \frac{1}{(\eta+\Delta)}\chi'\right) + \frac{\Delta}{(\eta+\Delta)}(\xi s\chi') + \frac{\Delta}{(\eta+\Delta)}(f\chi') - Kr(1+\delta\theta)^n \exp\left(\frac{-E}{(1+\delta\theta)}\right)\chi - \frac{\Delta}{(\eta+\Delta)}(\xi f' z) = 0. \tag{21}$$

The BCs are reduced as follows:

$$f' = 1, f + \xi q = 0, \theta' = Bi_1(\theta - 1), \chi' = Bi_2(\chi - 1).$$
$$f' \to 0, f'' \to 0, \theta \to 0, \chi \to 0. \tag{22}$$

The derivative of equations (18) through (21) and the corresponding boundary conditions (22) with regard to ξ are as follows:

$$q' = \frac{1}{\eta+\Delta} 2f's', \tag{23}$$

$$\frac{1+\beta_1}{1+\beta_2}\left(s''' + \frac{1}{(\eta+\Delta)}s'' - \frac{1}{(\eta+\Delta)^2}s'\right) - Ms' + \frac{Gr}{\xi}t - \frac{Gr}{\xi^2}\theta + \frac{\Delta}{(\eta+\Delta)^2}(\xi ss' + 2sf' + fs') + \frac{\Delta}{(\eta+\Delta)}(\xi ss'' + 2sf'' + fs'') - \frac{\Delta}{(\eta+\Delta)}(2f's' + s'f' + \xi(s')^2) = \frac{\Delta}{(\eta+\Delta)}(2q+q), \tag{24}$$

$$\frac{1}{\mathrm{Pr}}\left(t'' + \frac{1}{(\eta+\Delta)}t'\right) + \frac{\Delta}{(\eta+\Delta)}(\xi st' + s\theta') + \frac{\Delta}{(\eta+\Delta)}(s\theta' + ft') - \frac{\Delta}{(\eta+\Delta)}(\xi s't + f't) + \lambda Krn(1+\delta\theta)^{n-1}\delta t \exp\left(\frac{-E}{(1+\delta\theta)}\right)\chi + \lambda Kr(1+\delta\theta)^n \exp\left(\frac{-E}{(1+\delta\theta)}\right)\frac{1}{(1+\delta\theta)^2}E\delta t\chi + \lambda Kr(1+\delta\theta)^n \exp\left(\frac{-E}{(1+\delta\theta)}\right)z = 0, \tag{25}$$

$$\frac{1}{Sc}\left(z'' + \frac{1}{(\eta+\Delta)}z'\right) + \frac{\Delta}{(\eta+\Delta)}(\xi sz' + s\chi') + \frac{\Delta}{(\eta+\Delta)}(s\chi' + fz') - \frac{\Delta}{(\eta+\Delta)}(\xi s'z + f'z) - Kr\,(1+\delta\theta)^{n-1}n\delta t \exp\left(\frac{-E}{(1+\delta\theta)}\right)\chi - Kr(1+\delta\theta)^n \exp\frac{E\delta t}{(1+\delta\theta)^2}\left(\frac{-E}{(1+\delta\theta)}\right)\chi$$

$$- Kr(1+\delta\theta)^n \exp\left(\frac{-E}{(1+\delta\theta)}\right) z = 0. \tag{26}$$

The BCs are simplified as follows

$$s' = 1, s = 0, t' = Bi_1(t), z' = Bi_2(z).$$

$$s' \to 0, s'' \to 0, t \to 0, z \to 0. \tag{27}$$

After taking q out of equations (23) and (24), we get

$$\begin{aligned}
&\frac{1+\beta_1}{1+\beta_2}\left(s'''' + \frac{2}{(\eta+\Delta)}s''' - \frac{1}{(\eta+\Delta)^2}s'' + \frac{1}{(\eta+\Delta)^3}s'\right) \\
&- M\left(s'' + \frac{s'}{\eta+\Delta}\right) + \frac{Gr}{\xi}\left(t' + \frac{t}{\eta+\Delta}\right) \\
&- \frac{Gr}{\xi^2}\left(\theta' + \frac{\theta}{\eta+\Delta}\right) + \frac{\Delta}{(\eta+\Delta)^2}(\xi ss'' + \xi(s')^2 - 3f's' - s''f - 2f''s) \\
&+ \frac{\Delta}{(\eta+\Delta)}(\xi ss''' - \xi s's'' - f''s' + 2sf''' + fg''' - 2f's'') \\
&- \frac{\Delta}{(\eta+\Delta)^3}(s'f + 2f's + \xi s's) = 0.
\end{aligned} \tag{28}$$

The previously stated boundary layer equations for momentum, energy, and concentration, as well as the associated boundary conditions and auxiliary equations,

$$\begin{aligned}
&\left(f'''' + \frac{2}{(\eta+\Delta)}f''' - \frac{1}{(\eta+\Delta)^2}f'' + \frac{1}{(\eta+\Delta)^3}f'\right)\frac{1+\beta_1}{1+\beta_2} \\
&- M\left(f'' + \frac{f'}{\eta+\Delta}\right) + \frac{Gr}{\xi}\left(\theta' + \frac{\theta}{\eta+\Delta}\right) \\
&+ \frac{\Delta}{(\eta+\Delta)^3}(-ff' - \xi sf') - \frac{\Delta}{(\eta+\Delta)^2}(-\xi s'f' + 2(f')^2 - \xi f''s - ff'') \\
&+ \frac{\Delta}{(\eta+\Delta)}(ff''' - f''f' + \xi sf''' - \xi f's'') = 0.
\end{aligned} \tag{29}$$

$$\begin{aligned}
&\left(s'''' + \frac{2}{(\eta+\Delta)}s''' - \frac{1}{(\eta+\Delta)^2}s'' + \frac{1}{(\eta+\Delta)^3}s'\right)\frac{1+\beta_1}{1+\beta_2} \\
&- M\left(s'' + \frac{s'}{\eta+\Delta}\right) + \frac{Gr}{\xi}\left(t' + \frac{t}{\eta+\Delta}\right) \\
&- \frac{Gr}{\xi^2}\left(\theta' + \frac{\theta}{\eta+\Delta}\right) + \frac{\Delta}{(\eta+\Delta)^2}(\xi ss'' + \xi(s')^2 - 3f's' - s''f - 2f''s) \\
&+ \frac{\Delta}{(\eta+\Delta)}(\xi ss''' - \xi s's'' - f''s' + 2sf''' + fg''' - 2f's'') \\
&- \frac{\Delta}{(\eta+\Delta)^3}(s'f + 2f's + \xi s's) = 0.
\end{aligned} \tag{30}$$

$$\frac{1}{\mathrm{Pr}}\left(\theta'' + \frac{1}{(\eta+\Delta)}\theta'\right) + \frac{\Delta}{(\eta+\Delta)}(\xi s\theta') + \frac{\Delta}{(\eta+\Delta)}(f\theta') - \frac{\Delta}{(\eta+\Delta)}(\xi f' t) + \lambda Kr(1+\delta\theta)^n \exp\left(\frac{-E}{(1+\delta\theta)}\right)\chi = 0, \tag{31}$$

$$\frac{1}{\mathrm{Pr}}\left(t'' + \frac{1}{(\eta+\Delta)}t'\right) + \frac{\Delta}{(\eta+\Delta)}(\xi st' + s\theta') + \frac{\Delta}{(\eta+\Delta)}(s\theta' + ft') - \frac{\Delta}{(\eta+\Delta)}(\xi s't + f't) + \lambda Krn(1+\delta\theta)^{n-1}\delta t \exp\left(\frac{-E}{(1+\delta\theta)}\right)\chi + \lambda Kr(1+\delta\theta)^n \exp\left(\frac{-E}{(1+\delta\theta)}\right)\frac{1}{(1+\delta\theta)^2}E\delta t\chi + \lambda Kr(1+\delta\theta)^n \exp\left(\frac{-E}{(1+\delta\theta)}\right)z = 0, \tag{32}$$

$$\frac{1}{Sc}\left(\chi'' + \frac{1}{(\eta+\Delta)}\chi'\right) + \frac{\Delta}{(\eta+\Delta)}(\xi s\chi') + \frac{\Delta}{(\eta+\Delta)}(f\chi') - Kr(1+\delta\theta)^n \exp\left(\frac{-E}{(1+\delta\theta)}\right)\chi - \frac{\Delta}{(\eta+\Delta)}(\xi f' z) = 0. \tag{33}$$

$$\frac{1}{Sc}\left(z'' + \frac{1}{(\eta+\Delta)}z'\right) + \frac{\Delta}{(\eta+\Delta)}(\xi sz' + s\chi') + \frac{\Delta}{(\eta+\Delta)}(s\chi' + fz') - \frac{\Delta}{(\eta+\Delta)}(\xi s'z + f'z) - nKr\,(1+\delta\theta)^{n-1}\delta t \exp\left(\frac{-E}{(1+\delta\theta)}\right)\chi - Kr(1+\delta\theta)^n \exp\frac{E\delta t}{(1+\delta\theta)^2}\left(\frac{-E}{(1+\delta\theta)}\right)\chi - Kr(1+\delta\theta)^n \exp\left(\frac{-E}{(1+\delta\theta)}\right)z = 0. \tag{34}$$

The boundary conditions for the aforementioned equations are as follows:

$$\begin{aligned} &f' = 1, f + \xi q = 0, f' \to 0, f'' \to 0,\\ &s' = 1, s = 0, s' \to 0, s'' \to 0,\\ &\theta' = Bi_1(\theta - 1), \theta \to 0,\\ &t' = Bi_1(t), t \to 0,\\ &\chi' = Bi_2(\chi - 1), \chi \to 0,\\ &z' = Bi_2(z), z \to 0. \end{aligned} \tag{35}$$

4. Results and Discussion

This work investigates the consequence of endothermic and exothermic reactions on the motion of Boger fluid across a CSS. Convective boundary conditions and the impact

of an MF are also considered. Appropriate transformations are applied to the PDEs to convert them into a non-similar form, which allows for their solution. After that, local non-similarity techniques are used to solve the resultant equations, with truncation occurring at the second order. This section elaborates on the physical relevance of flow parameters on velocity $\left(\frac{\partial}{\partial\eta}f(\xi,\eta)\right)$, concentration $(\chi(\xi,\eta))$ and temperature $(\theta(\xi,\eta))$ profile in order to thoroughly assess the model's practical applicability. It is intended to clarify the consequences of the MF parameter (M), thermal Biot number (Bi_1), solvent fraction parameter (β_1), chemical reaction rate parameter (Kr), exothermic/endothermic parameter (λ), Activation energy parameter (E), solutal Biot number (Bi_2), and Schmidt number (Sc) on the flow field.

The fluid velocity variation is examined in Figure 1 concerning the magnetic field parameter's intensity. Observably, this effect has a negative outcome in that there is an inverse connection between the magnetic field and the velocity distribution. A rise in magnetic field values corresponds to a fall in fluid velocity. Physically, when a magnetic field influences a moving fluid, the particles of the fluid are stimulated, which results in a counter force that reduces and slows the fluid's motion; additionally, this force, which was originally called the Lorentz force, is perpendicular to both the MF vector and the velocity vector. The velocity distributions for the β_1 parameter is displayed in Figure 2. Increasing the β_1 results in an improvement in the velocity distribution. The Grashof number impact on velocity profiles for heat transmission is shown in Figure 3. It can be perceived that raising the Grashof number values for heat transfer causes the velocity profiles to rise. The Grashof number for heat transmission is defined as the thermal buoyant force to viscous force ratio. In terms of physics, raising the Grashof number causes the thermal buoyancy force to rise and the viscous force to decrease, which increases the velocity profiles. It is crucial in identifying the heat transmission mechanism, especially in cases of natural convection. Comprehending the Grashof number is crucial for scientists and engineers working in a variety of sectors, as it aids in forecasting fluid behavior in natural convection situations, directing the development and enhancement of heat exchange systems, thermal control, and several other uses.

The thermal behavior resulting from chemical reaction parameters for exothermic and endothermic parameters are depicted in Figures 4 and 5, respectively. When two chemical species interact, endothermic reactions $(\lambda = -1)$ consume energy, whereas exothermic reactions $(\lambda = 1)$ create energy. This chemical reaction is referred to as isothermic if the ratio of energy release to absorption is equal to that of absorption, since all of the energy in the reaction is balanced. It indicates that the endothermic process lowers the temperature of the Boger fluid. The system absorbs energy during the endothermic process, which subsequently lowers the fluid's temperature and $\theta(\xi,\eta)$. If the system discharges heat into the environment, a chemical reaction is said to be exothermic. The heat of system is transported to the surroundings, raising their temperature. Figures 6 and 7 display the influence of activation energy for exothermic and endothermic parameters on temperature, respectively. Figure 6 illustrates that for exothermic reactions $(\lambda = 1)$, a little lowering influence of the temperature profile is detected for rising values of E; whereas markedly opposite effects are obtained for endothermic reactions. This is the temperature profile that rises as E values for the endothermic process $(\lambda = -1)$ grow. Activation energy is the least energy needed to initiate a chemical reaction. A reaction's activation energy is typically expressed in kilojoules per mole and represented by the symbol Ea. In an endothermic process, energy is extracted from the environment, often

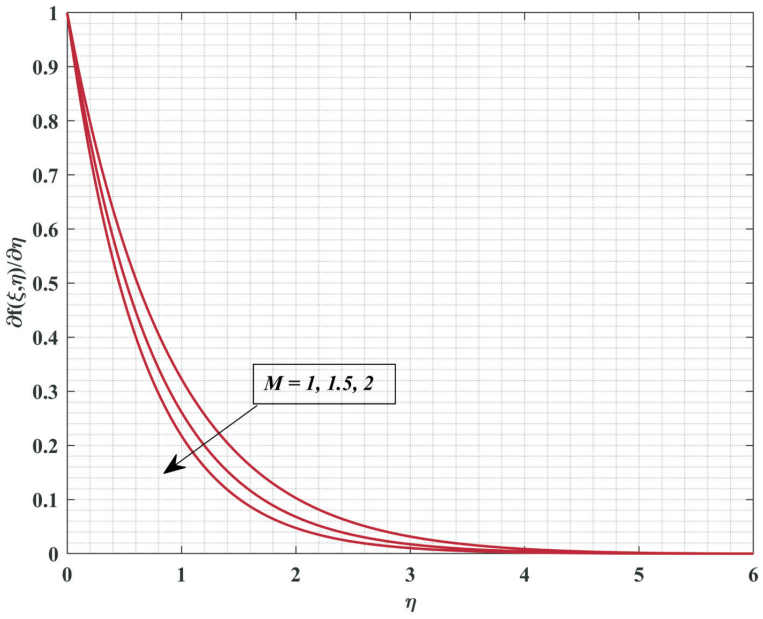

FIGURE 1. Plots of $\left(\frac{\partial}{\partial\eta}f(\xi,\eta)\right)$ for M.

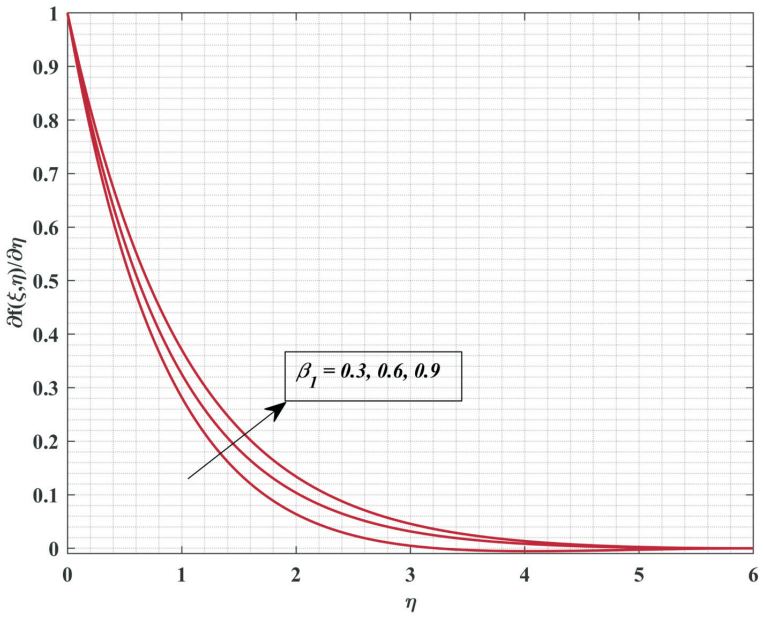

FIGURE 2. Plots of $\left(\frac{\partial}{\partial\eta}f(\xi,\eta)\right)$ for β_1.

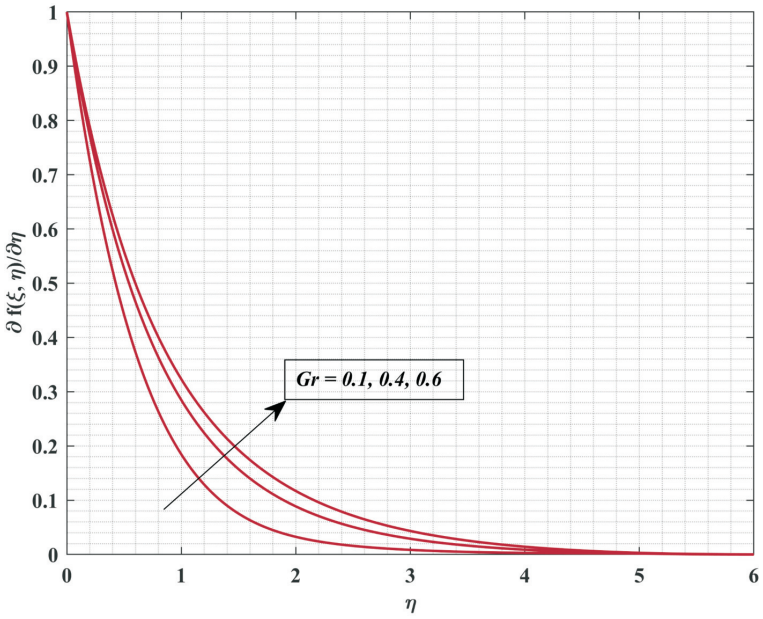

FIGURE 3. Plots of $\left(\frac{\partial}{\partial \eta} f(\xi, \eta)\right)$ for Gr.

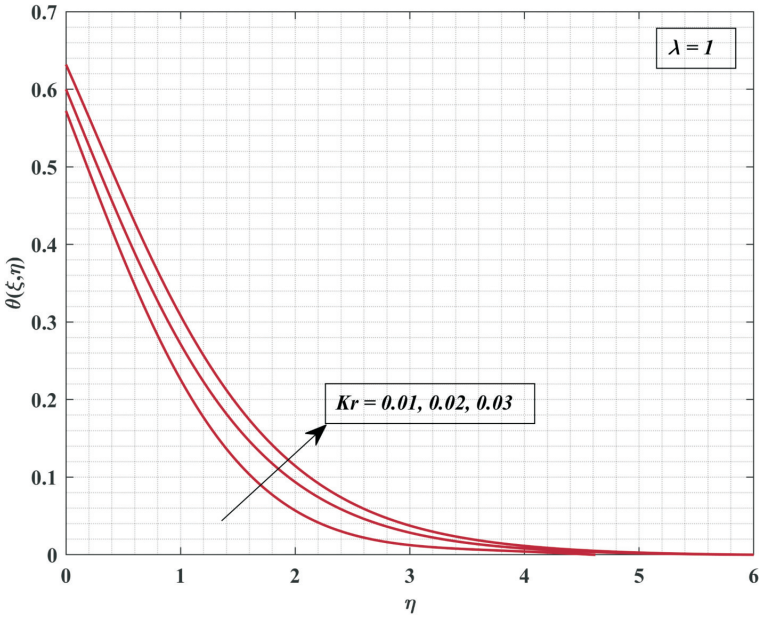

FIGURE 4. Plots of $\theta(\xi, \eta)$for Kr at $\lambda = 1$.

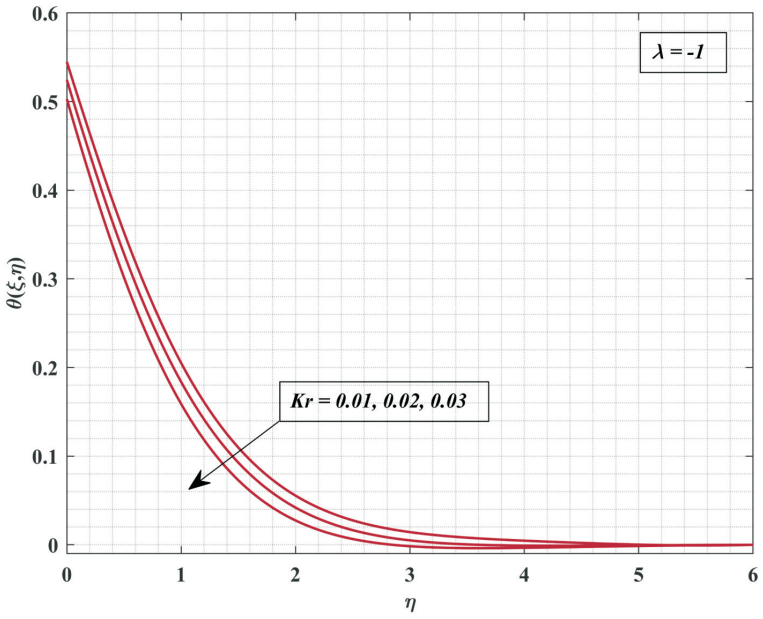

FIGURE 5. Plots of $\theta(\xi, \eta)$ for Kr at $\lambda = -1$.

from the liquid and surrounding solid surfaces. Furthermore, a lower reaction rate means that the liquid's endothermic reaction is producing less heat. The system's total thermal transmission is decreased as there is less heat available for transfer. As the activation energy parameter improves, so does the process's activation energy barrier. Still, in an exothermic case, this greater barrier consequences rather than stops the rate of heat transportation. Despite the greater activation energy barrier, the heat generated during the reaction is nonetheless transported to the neighboring solid and liquid systems. In this instance, a greater activation energy value could cause a slower reaction rate, but total heat transfer is still rather considerable once the reaction starts.

The examination of the $\theta(\xi, \eta)$ for different Bi_1 values is shown in Figure 8. The thermal Biot number Bi_1 exhibits an increasing response with thermal boundary layer thickness. The Biot number is a physical expression for the proportion of interior conductive heat transmission to surface convective heat transfer. The thermal boundary layer's thickness grows as the temperature of the surface escalates due to the intensified influence of the Bi_1, which characterizes surface convection. Since the heat transfer coefficient, or h_s, is involved in the Biot number, its value increases as h_s rises. As a result, increased heat transfer coefficient values result in increased temperature and thickness of the thermal boundary layer. The Biot number's capacity to provide information on the predominant mechanism of heat movement inside a system accounts for its physical relevance. Conduction is more prevalent when the object's interior resistance to heat conduction is significantly lower than the convective resistance at the surface, as shown by a small Biot number. Large Biot values indicate that convection is more prominent in the heat transfer process because the object's internal thermal resistance is larger than its surface convective resistance. Figure 9 presents the impact of solutal Biot number

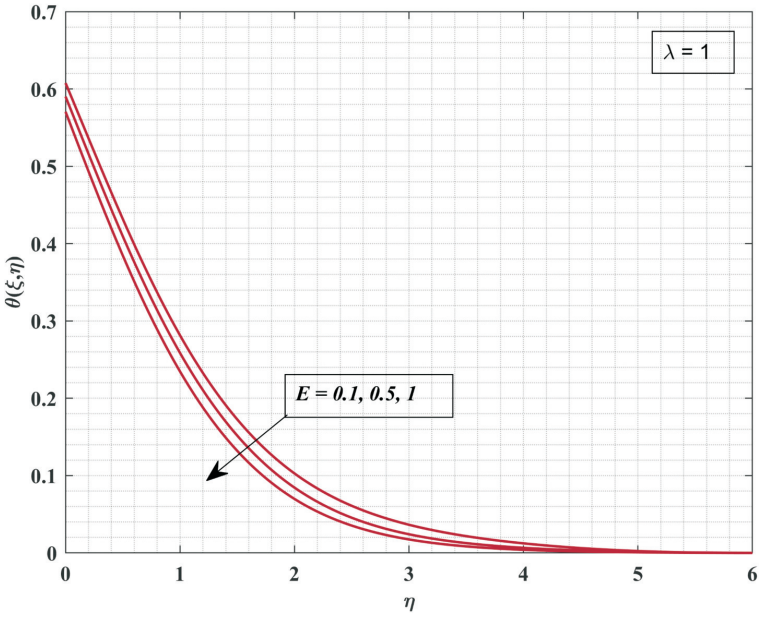

FIGURE 6. Plots of $\theta(\xi, \eta)$ for E at $\lambda = 1$.

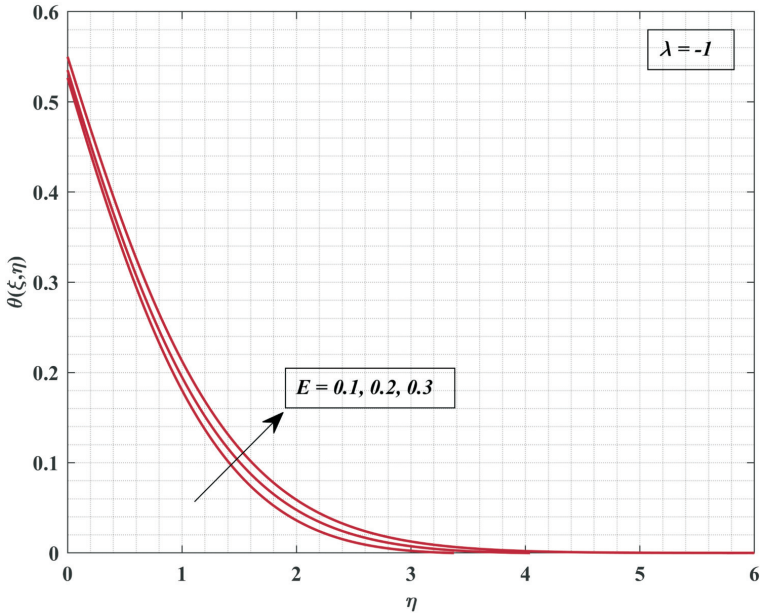

FIGURE 7. Plots of $\theta(\xi, \eta)$ for E at $\lambda = -1$.

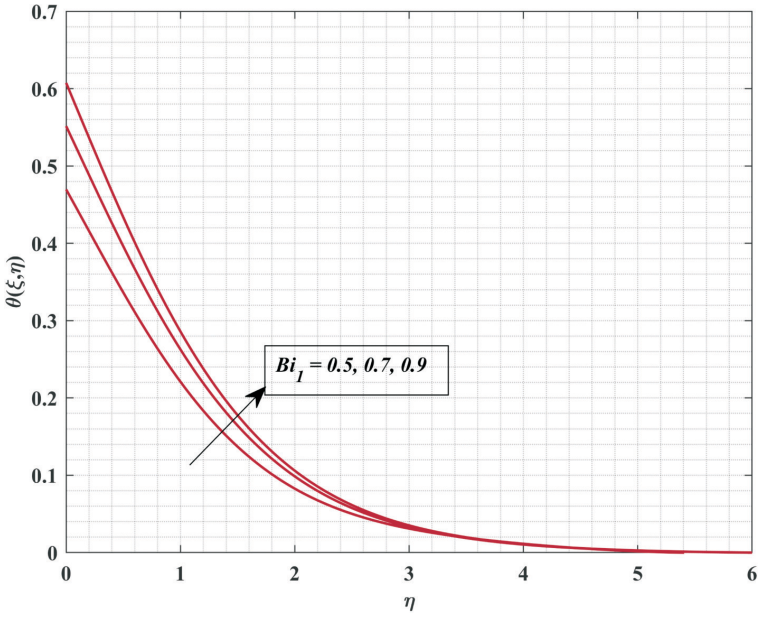

FIGURE 8. Plots of $\theta(\xi, \eta)$ for Bi_1.

(Bi_2) on $\chi(\xi, \eta)$. Increased Bi_2 causes $\chi(\xi, \eta)$ to expand. The solutal Biot number Bi_2 is expressed mathematically as the coefficient of mass-transference h_m, which increases as Bi_2 gets larger. Figure 10 illustrates the variation of chemical reaction factors on the $\chi(\xi, \eta)$. It is discovered that when the chemical reaction parameter increases, the species of concentration in the border layer decreases. This is because the chemical reaction in this system reduces the concentration by consuming the chemical. The most important impact is the chemical reaction's inclination to lessen overshoot in the solute concentration profiles in the solutal boundary layer. The significance of Eon the $\chi(\xi, \eta)$ is seen in Figure 11. The $\chi(\xi, \eta)$ rises for high values of E, as the graph demonstrates. Activation energy refers to the minimum quantity of energy necessary to initiate a reaction. Experimental evidence reveals that an increase in AE leads to a decline in the reaction rate constant, thereby causing a slowdown in the chemical process. The Arrhenius function deteriorates by increasing the E value, which proceeds to the generative chemical process being promoted and the concentration field being improved. A decreased reaction rate constant results from the combination of a high activation energy and a low temperature, which slows down the chemical reaction. This results in an elevation of the $\chi(\xi, \eta)$. The impact of Sc on the $\chi(\xi, \eta)$ is seen in Figure 12. It is observed that the $\chi(\xi, \eta)$ and the thickness of the solutal boundary layer diminish as the Sc rises. The Sc is really the ratio of mass diffusivity to momentum diffusivity. Higher Sc values are therefore associated with lower mass diffusivity. For this reason, when Sc increases, the penetration depth of the concentration function decreases. There is consensus that the concentration profile lowers as a result.

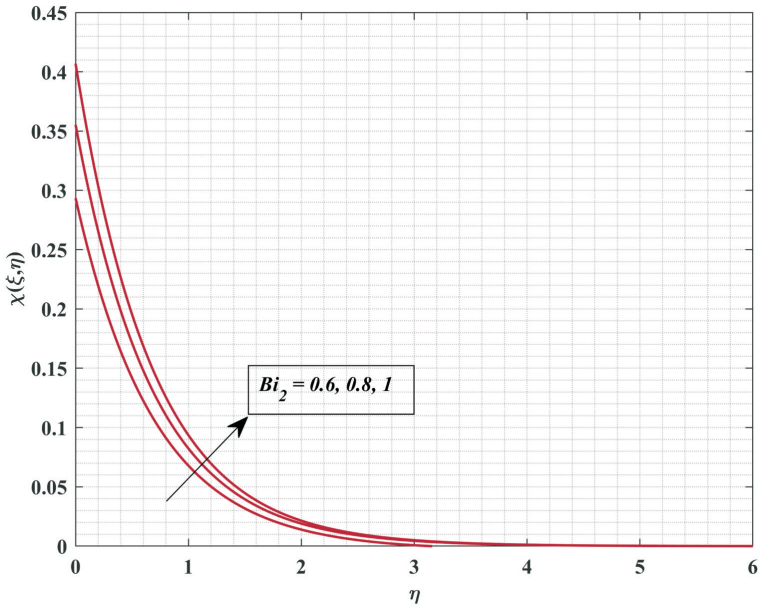

FIGURE 9. Plots of $\chi(\xi, \eta)$ for Bi_2.

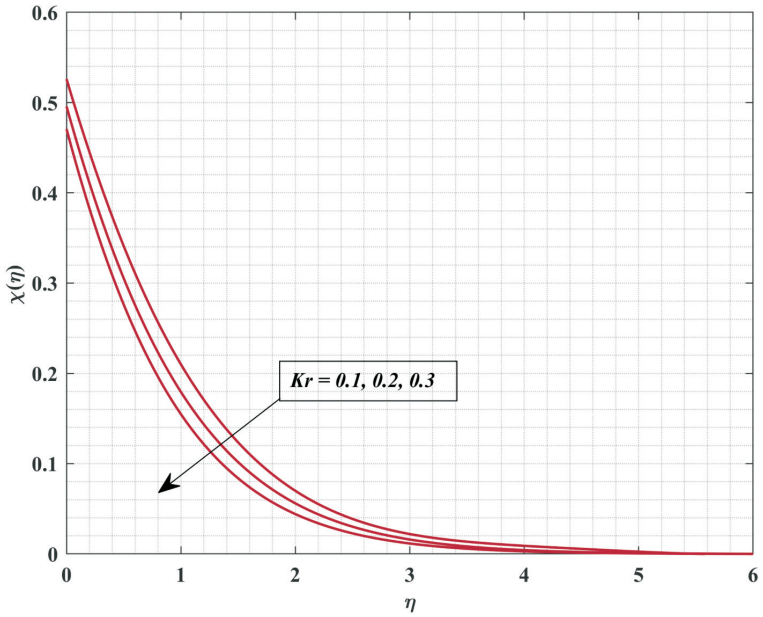

FIGURE 10. Plots of $\chi(\xi, \eta)$ for Kr.

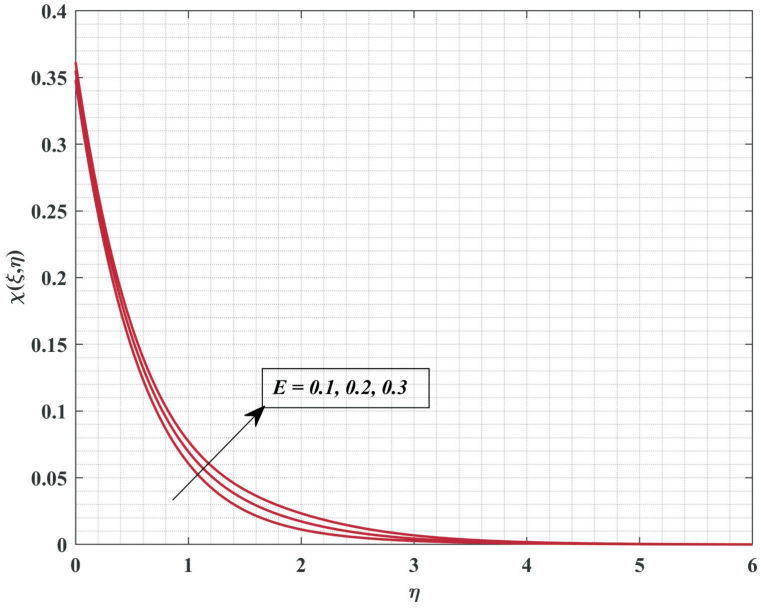

FIGURE 11. Plots of $\chi(\xi, \eta)$ for E.

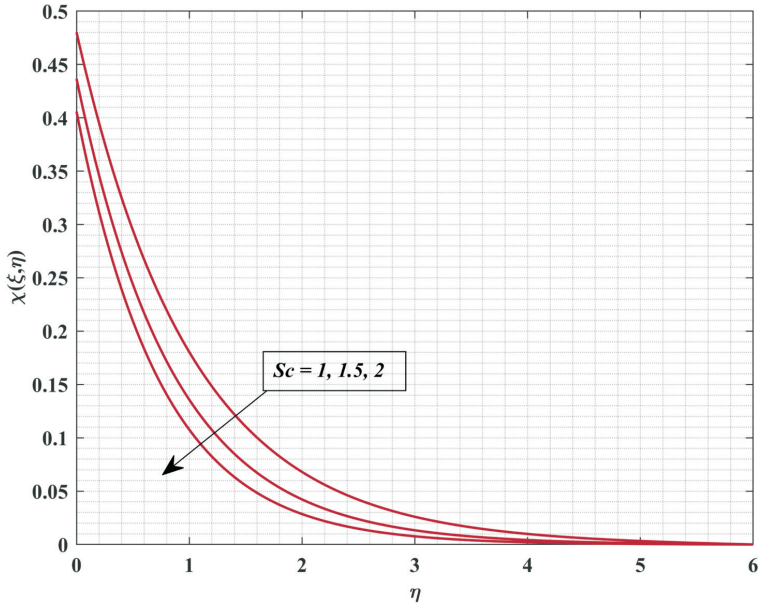

FIGURE 12. Plots of $\chi(\xi, \eta)$ for Sc.

5. Conclusion

This work investigates the stream of a Boger liquid past a CSS, considering the impact of a magnetic field and convective boundary conditions. Additionally, the properties of mass and heat transfer are studied through the application of exothermic and endothermic chemical processes. Using the proper non-similar transformations, the dimensional PDEs are transformed into dimensionless non-similar PDEs. The local non-similarity approach is then used to describe the dimensionless PDEs as a collection of ODEs. Graphs are used to examine how different factors affect the flow field. Some of the primary conclusions are as follows:

- $\frac{\partial}{\partial \eta} f(\xi, \eta)$ decays when the magnetic field parameter is augmented. This is because when a magnetic field influences a moving fluid, the particles of fluids are stimulated, which results in a Lorentz force that reduces and slows the fluid's motion.
- Increasing the Grashof number and solvent fraction parameter values increases the velocity distribution.
- For exothermic reactions, a little lowering influence of the temperature profile is detected for rising values of E; whereas markedly opposite effects are obtained for endothermic reactions.
- For exothermic processes, higher values of Kr show an increasing influence of the temperature profile; for endothermic reactions, the results are noticeably opposite.
- Both the thermal and concentration profile increases as the magnitude of thermal and solutal Biot numbers rise.
- The concentration profile decreases when the chemical reaction parameter and Schmidt number value escalate.
- As the activation energy parameters rise, the concentration profile likewise increases. The Arrhenius function declines as the AE increases, which precedes the generating chemical reaction being promoted, and the concentration field is improved.

Acknowledgments

Several anonymous reviewers provided thoughtful and detailed comments that greatly improved the final version of this article.

References

1. M. Abbas, N. Khan, M. S. Hashmi, F. M. Tawfiq, M. Inc and K. R. Raghunatha, *Numerical simulation of chemical reactive flow of Boger fluid over a sheet with heat source and local thermal non-equilibrium conditions*, Case Studies in Thermal Engineering, **59** (2024), Article Id: 104498, 17 Pages.
2. Z. Abbas, M. Naveed and M. Sajid, *Heat transfer analysis for stretching flow over a curved surface with magnetic field*, J. Engin. Thermophys., **22**(4) (2013), 337–345.
3. M. I. Afridi, Z.-M. Chen, N. Riaz and M. Qasim, *Heat transfer and flow analysis over a linearly stretching sheet with constant wall temperature: Novel local non-similar solutions in the presence of viscous heating*, ZAMM - Journal of Applied Mathematics and Mechanics/Zeitschrift für Angewandte Mathematik und Mechanik, 103(12) (2023), Article Id: e202300003.

4. V. R. Banakar, N. Patil, R. Kalia, B. Shankar and K. Karthik, *The role of nanoparticle diameter and solid-fluid interfacial layer behavior under low oscillating magnetic fields: A response surface methodology and ANOVA approach*, Proc. Inst. Mech. Eng. Part N J. Nanomater. Nanoeng. Nanosyst., 0(0) (2025), doi: 10.1177/23977914251341443.
5. V. R. Banakar, A. N. Mallikarjuna, P. Kattimani and A. Abdulrahaman, *Airfoil polynomials-based collocation approach to study time-varying fluid mechanism*, Int. Commun. Heat Mass Transf., **171** (2026), Article Id: 110105.
6. V. R. Banakar, N. K. R, P. Kattimani, B. Pattanayak and R. J. Punith Gowda, *Off-Centered Stagnation Point, Particle Movement, and Accumulation in a Chemically Reactive Fluid*, Chem. Eng. Technol., **49**(2) (2026), Article Id: e70166.
7. D. Dey and B. Chutia, *Modelling and Analysis of Dusty Fluid Flow Past a Vertical Surface with Exothermic and Endothermic Kind of Chemical Reactions*," in Advances in Thermofluids and Renewable Energy, P. Mahanta, P. Kalita, A. Paul and A. Banerjee, Eds., Singapore: Springer, (2022), 45–57.
8. D. Habib, N. Salamat, S. Hussain, S. Abdal, A. K. Hussein and B. Ali, *Variable viscosity effects on dynamic of non-Newtonian fluid nanofluid over a paraboloid of revolution via Keller box method*, Eur. Phys. J. Plus, **139**(5) (2024), Article Number: 427, 19 Pages.
9. T. Hayat, M. Rashid and A. Alsaedi, *MHD convective flow of magnetite-Fe3O4 nanoparticles by curved stretching sheet*, Results in Physics, **7** (2017), 3107–3115.
10. M. Imtiaz, F. Mabood, T. Hayat and A. Alsaedi, *Homogeneous-heterogeneous reactions in MHD radiative flow of second grade fluid due to a curved stretching surface*, International Journal of Heat and Mass Transfer, **145** (2019), Article Id: 118781.
11. S. Jagadha, D. Gopal, N. Patil, S. Singh, N. Kishan and S. K. Abhilasha, *Effect of higher order chemical reaction and Joule heating on rotational and permeable radiative MHD flow of Casson manganese ferrite fluid with heat generation/absorption*, Multiscale and Multidisciplinary Modeling, Experiments and Design, **8**(3) (2025), Article Number: 164, 18 Pages.
12. A. Jan, R. Nawaz and A. Ahmad, *Non-similar analysis of radially magnetized flow and heat transfer of Reiner–Philippoff based nanofluid over a curved stretching surface with viscous dissipation*, International Journal of Thermofluids, **22**(6) (2024), Article Id: 100657.
13. M. Kouki, I. Ullah, S. Ullah, M. Mahtab Alam, H. Khan and M. M. M. Abdou, Exploring the impact of thermal energy and exothermic-endothermic reactions on differential type fluid flow in a convergent/divergent channel, Case Studies in Thermal Engineering, **55** (2024), Article Id: 104163.
14. C. Liu, N. Shahmir, M. Ramzan, A. M. S. Alhuthali, C. A. Saleel and S. Kadry, *A non-similar solution to dissipative Eyring-Powell nanofluid flow over a nonlinear stretching surface with an inclined magnetic field and active/passive nanoparticles flux*, ZAMM - Journal of Applied Mathematics and Mechanics/Zeitschrift für Angewandte Mathematik und Mechanik, **104**(6) (2024), Article Id: e202300706.
15. A. N. Mallikarjuna, V. R. Banakar, A. Abdulrahman and R. S. V. Kumar, Study on thermophoretic deposition of particles and ratio of effective heat capacity: A collocation approach, Int. Commun. Heat Mass Transf., **169** (2025), Article Id: 109841.
16. M. Mansoor, S. Kamran, B. Ahmad and Q. Ul-Hassan, *Non-similar modelling of Williamson Fluid over a non-linear stretching sheet with temperature dependent thermal conductivity and Chemical Reactions*, ZAMM - Journal of Applied Mathematics and Mechanics/Zeitschrift für Angewandte Mathematik und Mechanik, **102**(11) (2022), Article Id: e202200118.
17. P. S. S. Nagalakshmi and N. Vijaya, *Three Dimensional Boger Nanofluid Flow Explored with Carbon Nanotubes Over a Riga Plate*, Journal of Nanofluids, **9**(2) (2020), 114–120.
18. M. Naveed, Z. Abbas and M. Sajid, *MHD Flow of Micropolar Fluid due to a Curved Stretching Sheet with Thermal Radiation*, Journal of Applied Fluid Mechanics, 9(1) (2015), 131–138.
19. S. Panda, R. Baithalu and S. R. Mishra, *Thermal characteristics of Boger-micropolar tri-hybrid nanofluid magnetized squeezing flow within concentric parallel discs*, Journal of Thermal Analysis and Calorimetry, 149 (2024), 13071–-13080.
20. K. Preethi, B. N. Hanumagowda, K. M. Pavithra, S. V. K. Varma, V. S. Mann, R. Singh, P. Kattimani, *Forchheimer flow of hybrid nanofluid over a stretching sheet with Richardson number and quadratic thermal radiation: hyperbolic tangent model*, **8**(3) (2025), Article Number 171, 15 Pages.

21. R. J. Punith Gowda, S. K. Abhilasha, N. Patil, R. Kalia and U. C. Kolli, *Comparison of horizontal magnetic field and uniform magnetic on the nanofluid flow in rough rotating disk system: A response surface methodology and ANOVA approach*, Proceedings of the Institution of Mechanical Engineers Part N Journal of Nanomaterials Nanoengineering and Nanosystems, (2026), Article Id: 23977914251404181, 15 Pages.
22. R. Raza, F. Mabood and R. Naz, *Entropy analysis of non-linear radiative flow of Carreau liquid over curved stretching sheet*, International Communications in Heat and Mass Transfer, **119** (2020), Article Id: 104975.
23. T. Sajid, M. K. Al Mesfer, W. Jamshed, M. R. Eid, M. Danish, K. Irshad, R. W. Ibrahim, S. Batool, S. M. El Din and G. C. Altamirano, *Endo/exothermic chemical processes influences of tri-hybridity nanofluids flowing over wedge with convective boundary constraints and activation energy*, Results in Physics, **51** (2023), Article Id: 106676.
24. B. K. Sharma, R. Gandhi, N. K. Mishra and Q. M. Al-Mdallal, *Entropy generation minimization of higher-order endothermic/exothermic chemical reaction with activation energy on MHD mixed convective flow over a stretching surface*, Scientific Reports, **12** (2022), Article Number: 17688.
25. I. Ullah, *Activation energy with exothermic/endothermic reaction and Coriolis force effects on magnetized nanomaterials flow through Darcy–Forchheimer porous space with variable features*, Waves in Random and Complex Media, 35(1) (2025), 398–-411.
26. Y. Veeranna, P. Kattimani, A. Kulshreshta, R. J. Punith Gowda and I. E. Sarris, *Significance of solvent percentage and external pollutant source concentration in Boger-micropolar fluid flow across a semi-circular body*, International Journal of Thermofluids, **29** (2025), Article Id: 101399, 10 Pages.
27. A. Yasmin, K. Ali and M. Ashraf, *Study of Heat and Mass Transfer in MHD Flow of Micropolar Fluid over a Curved Stretching Sheet*, Scientific Reports, **10** (2020), Article number: 4581.

S. Sureshkumar, Department of Mathematics, Siddaganga Institute of Technology, Tumukuru 572 103, India.
Email address: ssk@sit.ac.in

K. M. Devendraiah, Department of Mathematics, V. V. Sangha's Independent P U College, Ballari 583 104, Karnataka, India.
Email address: devendraiahkm@gmail.com

S. Prasanna Rani, Department of Mathematics, Government Degree College for Women, Begumpet, (Affiliated to Osmania University), Hyderabad 500 016, India.
Email address: prasanna211221@gmail.com

C. G. Jagannatha, Department of Mathematics, HPPC Government First Grade College, Challakere 577 501, Karnataka, India.
Email address: cgjagannath@gmail.com

Lal Sing Naik, Department of Mathematics, Government Science College, Chitradurga, Karnataka, India.
Email address: lsnaikchiru@gmail.com

K. C. Jagadeesha, Department of in Mathematics, Government First Grade College, Tumkur 572 102, Karnataka, India.
Email address: kcjagadish.09@gmail.com